Post-print of: Kozieł S., Unnsteinsson S., Bekasiewicz A.: On low-fidelity models for variable-fidelity simulation-driven design optimization of compact wideband antennas. 2018 22nd International Microwave and Radar Conference (MIKON). DOI: 10.23919/MIKON.2018.8404991

On Low-Fidelity Models for Variable-Fidelity Simulation-Driven Design Optimization of Compact Wideband Antennas

Slawomir Koziel[1], Sigmar D. Unnsteinsson[1]
[1]Engineering Optimization & Modeling Center
Reykjavik University
Reykjavik, Iceland
koziel@ru.is, sigmaru14@ru.is

Adrian Bekasiewicz[2]
[2]Faculty of Electronics, Telecommunications and Inf.
Gdansk University of Technology
Gdansk, Poland
bekasiewicz@ru.is

***Abstract*—The paper addresses simulation-driven design optimization of compact antennas involving variable-fidelity electromagnetic (EM) simulation models. Comprehensive investigations are carried out concerning selection of the coarse model discretization density. The effects of the low-fidelity model setup on the reliability and computational complexity of the optimization process are determined using a benchmark set of three ultra-wideband antennas designed for the best matching and for the minimum size. The optimization algorithm of choice is trust-region gradient search with low-fidelity model correction realized through frequency scaling and multiplicative output space mapping. The results indicate that appropriate low-fidelity model setup can be assessed using a correlation analysis based on the selected characteristic points of the antenna responses and sparsely allocated test designs, and the results are consistent across the considered benchmark set.**

Keywords*—Antenna design; EM-driven design; variable-fidelity simulations; design optimization; low-fidelity models

I. Introduction

Design of compact antennas has become an important research topic over the recent years [1]-[8]. This is primarily due to a growing number of applications in which maintaining a small size of the structure is critical, such as mobile handheld devices [1], wearable/implantable devices [2], or Internet of Things (IoT) [3], global navigation satellite systems [4], or microwave imaging [6]. Miniaturization of antennas faces some fundamental challenges, some of which are related to physical limitations, others pertinent to topological complexity of the structures.

On the physical side, reduction of antenna dimensions normally leads to a degradation of both electrical and field characteristics. In case of wideband and ultra-wideband antennas, it is mostly articulated through difficulties in maintaining required impedance bandwidth [9], deterioration of gain (increased in-band gain variability) and efficiency. On the other hand, miniaturization may lead to improvement of time domain performance (e.g., pulse fidelity [10]) as well as pattern stability [10]. Due to performance specifications imposed on the antenna, practical designs are always trade-offs between the conflicting objectives, one of which being size reduction. From optimization perspective, some of the performance constraints (e.g., maximum in-band reflection level) are always active at the optimum design.

Topological changes permit partial workaround to size limitations of small antennas. Popular modifications include re-shaping of the radiator [11], [12], incorporating ground plane slits [13] and stubs [14], employing defected ground structures (DSG) [15], extending current paths by meandering radiator edges [16], utilization of transversal signal-interference feeds [17], or loading with grounded strips [18]. From the point of view of a design process, there are several important issues that arise here: (i) increasing geometrical complexity of the structures and increasing the number of parameters that need to be adjusted, (ii) necessity of simultaneous tuning of all relevant antenna parameters (which rules out parameter sweeping as reliable design approach) [9], [19], and (iii) increasing computational cost of performance evaluation. While full-wave EM analysis is mandatory for design closure of compact antennas, complex geometries increase cost of the process.

Due to all of the aforementioned factors, EM-driven compact antenna optimization is not trivial. In particular, utilization of conventional optimization algorithms (both local [20], and global, especially population-based metaheuristics [21]) is often hindered by their prohibitive CPU cost. Computationally feasible optimization can be realized by exploiting adjoint sensitivities [22], as well as surrogate-assisted methods [19]. Techniques of this class may involve data-driven models (e.g., kriging interpolation [23]) or physics-based ones (e.g., response correction methods [24], feature-based optimization [25]). An important issue pertinent to surrogate methods is selection of the underlying low-fidelity models, which, in case of antennas, are most often based on coarse-discretization EM simulations.

In this paper, we conduct a study concerning the low-fidelity model setup for compact wideband antenna design. Models of different discretization densities are considered and utilized by a surrogate-assisted optimization algorithm with the design objectives imposed on improvement of antenna matching, as well as its size reduction. The effect of particular low-fidelity model choice on the performance of the optimization process is studied both in the context of its reliability and the computational cost. Numerical tests are performed using three ultra-wideband (UWB) compact antennas. The results indicate that appropriate discretization density can be determined using simple and cheap statistical analysis carried out before optimization.

II. Low-Fidelity Models of Compact Antennas

Low-fidelity computational models are often utilized in order to reduce the cost of the simulation-driven optimization process [19]. As indicated in [26], selecting appropriate model discretization density may be critical for optimization algorithm performance, both in terms of its reliability, and computational complexity. For specific types of surrogate-assisted algorithms, it is possible to automatically determine the optimum mesh density through correlation analysis [27], however, the problem is still open in a general case.

Here, we consider a particular class of antennas, which are compact ultra-wideband structures. Figure 1 shows an example of a UWB monopole and reflection characteristics corresponding to the high-fidelity model $\boldsymbol{R}_f$ and several low-fidelity models of various discretization densities. It can be observed that some of these models are clearly too coarse while other seem appropriate at a first glance. On the other hand, achieving sufficient model correlation (critical for algorithm performance) is difficult to be assessed visually. A comprehensive numerical study for a particular optimization algorithm (cf. Section III) has been provided in Section IV with the objective being determination of the most advantageous low-fidelity model selection.

Furthermore, a simple analysis is utilized to determine correlation between the low- and high-fidelity models as a mean to find low-fidelity model of sufficient quality (i.e., the one that permits reliable design optimization). Figure 2 shows example antenna responses along with selected characteristic points as described in the figure caption. Let $\boldsymbol{L}_f^{(k)} = [l_{f.1}^{(k)} \ldots l_{f.p}^{(k)}]$ and $\boldsymbol{L}_c^{(k)} = [l_{c.1}^{(k)} \ldots l_{c.p}^{(k)}]$ denote levels of the characteristic points corresponding to the local maxima of the responses at the design $\boldsymbol{x}^{(k)}$, $k = 1, \ldots, K$. For the sake of correlation analysis the designs $\boldsymbol{x}^{(k)}$ are allocated randomly within the design space. Let $\boldsymbol{dL}^{(k)} = [dL_1^{(k)} \ldots dL_p^{(k)}] = \boldsymbol{L}_f^{(k)} - \boldsymbol{L}_c^{(k)}$, and σ_j are standard deviations of vectors $[dL_j^{(1)} \ldots dL_j^{(K)}]$. We define the correlation factor as $\sigma = (\sum_{j=1,\ldots,p} \sigma_j)/p$. It indicates averaged discrepancy between the low- and high-fidelity models (it is zero for no discrepancy and grows with increasing discrepancy). One of the objectives is to find out whether any universal threshold for σ can be found that ensures design process reliability when using a particular low-fidelity model within a variable-fidelity optimization framework.

III. Optimization Algorithm

In this section, a short outline of the optimization algorithm utilized in our numerical studies is provided. We describe the correction procedure of the low-fidelity model and briefly describe a surrogate-based trust-region gradient search algorithm (the main optimization engine).

A. Low-Fidelity Model Correction

The low-fidelity model correction utilized here is nonlinear frequency scaling and multiplicative response correction. Let $\boldsymbol{R}_c(\boldsymbol{x}) = [R_c(\boldsymbol{x},f_1) \ \ R_c(\boldsymbol{x},f_2) \ \ \ldots \ \ R_c(\boldsymbol{x},f_m)]^T$, where $R_c(\boldsymbol{x},f_k)$ is evaluation of the low-fidelity model at frequency f_k (here, $|S_{11}|$). The frequency-scaled model $\boldsymbol{R}_{c.F}(\boldsymbol{x})$ is defined as

$$\boldsymbol{R}_{c.F}(\boldsymbol{x}) = [R_c(\boldsymbol{x}, F_0 + F_1 f_1 + F_2 f_1^2) \ \ldots \ R_c(\boldsymbol{x}, F_0 + F_1 f_m + F_2 f_m^2)]^T \quad (1)$$

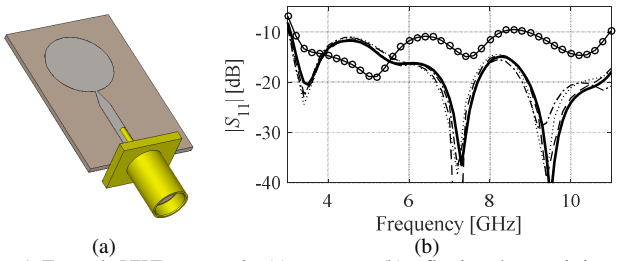

(a) (b)

Fig. 1. Example UWB monopole: (a) geometry, (b) reflection characteristics of the high-fidelity model (—), and low-fidelity model with LPW = 10 (– ○), LPW = 12 (– · –), LPW = 14 (···), LPW = 16 (– –). Here, LPW is a lines-per-wavelength parameters utilized by CST Microwave Studio (a global mesh parameter).

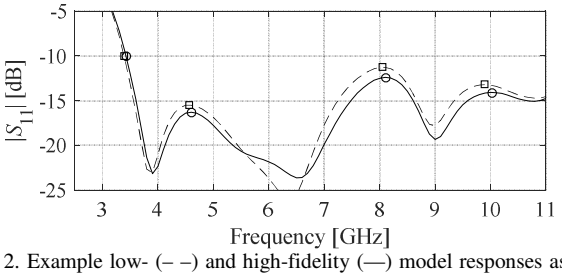

Fig. 2. Example low- (– –) and high-fidelity (—) model responses as well as selected characteristic points (here, corresponding to –10 dB level at the lower end of the operational bandwidth as well as local maxima of the responses).

Here, F_k, $k = 0, 1, 2$, are scaling parameters obtained to minimize the misalignment between $\boldsymbol{R}_{c.F}$ and $\boldsymbol{R}_f$ at $\boldsymbol{x}^{(i)}$ as

$$[F_0, F_1, F_2] = \arg\min_{[F_0,F_1,F_2]} \| \boldsymbol{R}_f(\boldsymbol{x}^{(i)}) - \boldsymbol{R}_{c.F}(\boldsymbol{x}^{(i)}) \| \quad (2)$$

The multiplicative response correction is implemented as

$$\boldsymbol{R}_s^{(i)}(\boldsymbol{x}) = \boldsymbol{A} * \boldsymbol{R}_{c.F}(\boldsymbol{x}^{(i)}) \quad (3)$$

where $\boldsymbol{A} = \boldsymbol{R}_f(\boldsymbol{x}^{(i)}) // \boldsymbol{R}_{c.F}(\boldsymbol{x}^{(i)})$, where // and * denote component-wise division and multiplication, respectively. It should be noted that the computational cost of computing correction coefficients is negligible. In particular, the frequency-scaled low-fidelity model response $\boldsymbol{R}_c(\boldsymbol{x}, F_0 + F_1 f_k + F_2 f_k^2)$, $k = 1, \ldots, m$, is obtained by interpolating $\boldsymbol{R}_c(\boldsymbol{x}, f_k)$.

B. Problem Formulation and Optimization Algorithm

Given the high-fidelity antenna model $\boldsymbol{R}_f(\boldsymbol{x})$ with $\boldsymbol{x}$ being adjustable parameters, the design problem is formulated as

$$\boldsymbol{x}^* = \arg\min_{\boldsymbol{x}} U(\boldsymbol{R}_f(\boldsymbol{x})) \quad (4)$$

where U is an objective function that encodes given performance specifications; $\boldsymbol{x}^*$ is the optimum design to be found. The problem (4) is solved using a generic trust-region-embedded surrogate-assisted scheme

$$\boldsymbol{x}^{(i+1)} = \arg\min_{\boldsymbol{x}; \|\boldsymbol{x} - \boldsymbol{x}^{(i)}\| \le \delta^{(i)}} U(\boldsymbol{R}_s^{(i)}(\boldsymbol{x})) \quad (5)$$

where $\boldsymbol{R}_s^{(i)}$ is obtained as in (1)-(3), and $\delta^{(i)}$ is a trust-region radius. The latter is updated after each iteration. Note that $\boldsymbol{R}_s^{(i)}(\boldsymbol{x}^{(i)}) = \boldsymbol{R}_f(\boldsymbol{x}^{(i)})$ by the definition of the surrogate. The surrogate is reset after each successful iteration of (5).

C. Objective Function

Here, we consider two cases: (i) optimization for best matching, and (ii) optimization for minimum size with the

constraint on antenna reflection (i.e., to keep $|S_{11}| \le -10$ dB in the UWB range). The objective function for the first case is defined as

$$U(\boldsymbol{R}_f(\boldsymbol{x})) = S(\boldsymbol{x}) \tag{6}$$

where $S(\boldsymbol{x})$ is the maximum in-band reflection. The objective for the second case is defined as

$$U(\boldsymbol{R}_f(\boldsymbol{x})) = A(\boldsymbol{x}) + \beta \cdot c(S(\boldsymbol{x}))^2 \tag{7}$$

where $A(\boldsymbol{x})$ is the antenna footprint, β is a penalty factor (here, $\beta = 1000$), and c is a penalty function defined as $c(S(\boldsymbol{x})) = \max\{(S(\boldsymbol{x})+10)/10, 0\}$. The penalty function is a relative violation of the condition $|S_{11}| \le -10$ dB in the UWB band.

IV. Case Studies and Results

A. Test Cases and EM Models

In our numerical study, we consider three UWB antenna structures. The first structure (Antenna I) is a monopole antenna with two radiator slots and an elliptical slit below the feed line [28]. The design parameters are $\boldsymbol{x}_\text{I} = [L_g\ L_0\ L_s\ W_s\ d\ dL\ d_s\ dW_s\ dW\ a\ b]^T$. The second structure (Antenna II) consists of a circular patch fed through a tapered 50 Ohm microstrip line and modified ground plane with L-shaped strip aimed at enhancement of the current path within the compact geometry [29]. The design variables are: $\boldsymbol{x}_\text{II} = [w_0\ l_1\ l_2\ l_3\ l_4\ w_1\ w_2\ w_3\ r\ o_r]^T$, whereas parameters $w_f = 1.7$, $l_f = 10$ and $o = 0.5w_0 \cdot r \cdot o_r$ (all dimensions in mm). The last structure (Antenna III) consists of a driven element in the form of a trapezoid radiator fed through a microstrip line. The geometry is described by the following set of design parameters: $\boldsymbol{x}_\text{III} = [l_0\ l_1\ w_{1r}\ w_2\ o_{2r}\ o_{3r}\ s_{1r}\ s_{2r}\ s_{4r}\ s_{5r}]^T$. Relative variables are $w_1 = (0.5w_2 - 0.5w_0)w_{1r}$, $o_2 = 0.5w_2o_{2r}$, $o_3 = (l_1 - s_3)o_{3r}$, $s_1 = (0.5w_2 - 0.5w_0)s_{1r}$, $s_2 = l_1s_{2r}$, $s_4 = (w_2 - 2s_5)s_{4r}$, and $s_5 = 0.5(l_0 - g)s_{5r}$. Parameters $w_0 = 1.7$, $o_1 = 0.25$, $g = 0.5$ remain fixed. Geometries of all antennas are shown in Fig. 3. Antenna I is implemented on Rogers RO4003 substrate ($\varepsilon_r = 3.55$, $h = 0.813$ mm). Antennas II and III are implemented on a 0.762 mm thick Taconic RF-35 dielectric substrate ($\varepsilon_r = 3.5$, $\tan\delta = 0.0018$). The EM models are implemented in CST Microwave Studio and simulated using its time domain solver. The details concerning the models have been provided in Table I.

B. Optimization Results

Antennas I through III have been optimized for best matching and for minimum size using the objective functions (6) and (7), respectively. The results have been gathered in Tables II, III, and IV, as well as shown in Fig. 4. It can be observed that—for each antenna—there is certain minimum value of LPW beyond which the optimization process becomes unreliable, either because of premature convergence (due to shrinking of the trust region size) or simply poor results obtained. This occurs for LPW of around 12 for the first two cases, and around 14 for the last case. The results of statistical analysis shown in Table I indicate that the corresponding value of σ is around 0.5, which can be considered as a reasonable threshold value for the low-fidelity model. Operating around this threshold permits reliable optimization at possibly low computational cost.

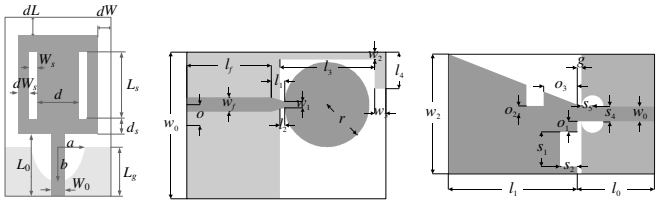

Fig. 3. Benchmark antennas: (a) Antenna I [28], (b) Antenna II [29], (c) Antenna III [30].

TABLE I EM Models for UWB Antennas of Fig. 2

Model	Antenna I		Antenna II		Antenna III	
	Time# [s]	$\sigma$$	Time# [s]	$\sigma$$	Time# [s]	$\sigma$$
High-Fidelity	1,518	N/A	1,244	N/A	1,936	N/A
Low-fidelity, LPW = 8	58	∝	47	∝	40,1	∝
Low-fidelity, LPW = 9	65	0.76	51	∝	43,3	∝
Low-fidelity, LPW = 10	76	0.67	59	1.70	47,8	∝
Low-fidelity, LPW = 11	84	0.45	62	0.55	49,9	1.67
Low-fidelity, LPW = 12	103	0.33	89	0.41	61,5	0.95
Low-fidelity, LPW = 14	166	0.37	135	0.33	92,5	0.42
Low-fidelity, LPW = 16	210	0.28	177	0.29	144,5	0.32
Low-fidelity, LPW = 18	283	0.25	220	0.16	199,3	0.31
Low-fidelity, LPW = 20	512	0.22	315	0.14	352,3	0.21

Average simulation time.
$ Symbol ∝ means that response is severely distorted (compared to that of the high-fidelity model) and respective characteristic points do not exist.

TABLE II Optimization Results for Antenna I

Objective function	Cost and performance	Low-fidelity model LPW								
		8	9	10	11	12	14	16	18	20
(6) [best matching]	$S(\boldsymbol{x}^*)$	–6.9	–9.0	–13.7	–12.6	–12.9	–11.8	–13.6	–11.8	–14.1
	# of $\boldsymbol{R}_f$	8	8	13	15	14	18	16	12	13
	# of $\boldsymbol{R}_c$	74	96	123	158	124	172	137	78	112
	Total [h]	4.6	5.0	8.1	10.0	9.5	15.5	14.7	11.2	21.4
(7) [size reduction]	$A(\boldsymbol{x}^*)$	401	463	462	330	346	265	225	241	296
	# of $\boldsymbol{R}_f$	7	8	19	11	15	14	20	15	16
	# of $\boldsymbol{R}_c$	40	41	129	66	158	91	174	103	93
	Total [h]	3.6	4.1	10.7	6.2	10.8	10.1	18.6	14.2	19.9

TABLE III Optimization Results for Antenna II

Objective function	Cost and performance	Low-fidelity model LPW								
		8	9	11	11	12	14	16	18	20
(6) [best matching]	$S(\boldsymbol{x}^*)$	–8.9	–10.0	–12.7	–8.2	–16.7	–17.5	–16.5	–17.1	–16.1
	# of $\boldsymbol{R}_f$	8	8	8	8	11	12	10	13	12
	# of $\boldsymbol{R}_c$	48	38	68	58	81	72	50	73	72
	Total [h]	3.4	3.3	4.9	3.8	5.8	6.8	5.9	8.9	10.4
(7) [size reduction]	$A(\boldsymbol{x}^*)$	707	699	723	671	557	471	627	529	567
	# of $\boldsymbol{R}_f$	20	20	3	7	13	13	13	20	19
	# of $\boldsymbol{R}_c$	170	220	33	37	63	63	63	110	120
	Total [h]	9.1	10.0	1.6	3.1	6.0	6.9	7.6	13.6	17.1

TABLE IV Optimization Results for Antenna III

Objective function	Cost and performance	Low-fidelity model LPW								
		8	9	11	11	12	14	16	18	20
(6) [best matching]	$S(\boldsymbol{x}^*)$	–10.9	–8.2	–10.5	–8.6	–11.0	–9.7	–12.3	–11.4	–11.2
	# of $\boldsymbol{R}_f$	13	7	11	7	10	8	14	14	19
	# of $\boldsymbol{R}_c$	109	55	95	31	70	44	98	134	163
	Total [h]	8.2	4.4	7.2	4.2	6.6	5.4	11.5	14.9	26.2
(7) [size reduction]	$A(\boldsymbol{x}^*)$	309	321	293	289	317	295	309	302	307
	# of $\boldsymbol{R}_f$	14	9	10	8	15	11	17	12	12
	# of $\boldsymbol{R}_c$	122	45	46	32	87	59	125	72	120
	Total [h]	8.9	5.4	6.0	4.7	9.6	7.4	14.2	10.4	18.2

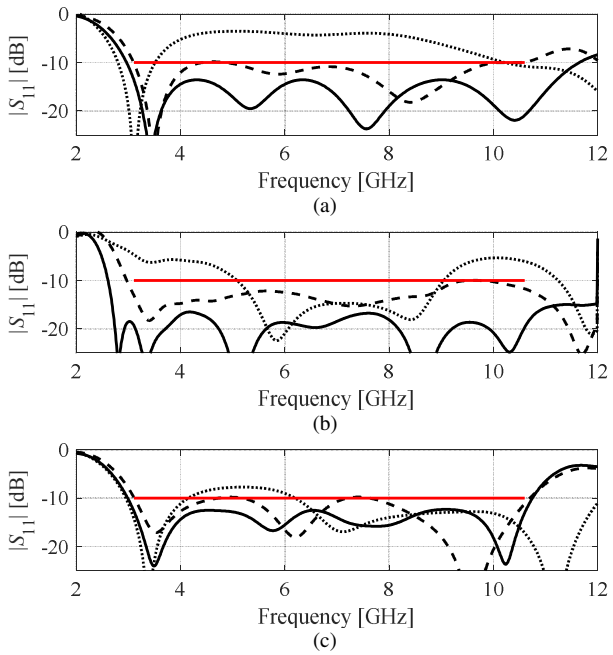

Fig. 4. Reflection responses of the optimized antennas; initial design (····), optimization for best matching (—), and optimization for size (- - -): (a) Antenna I, (b) Antenna II, (c) Antenna III. Results for LPW = 16. Maximum in-band reflection for size-optimized antennas are at –10 dB level as expected.

V. Conclusion

In the paper, the problem of low-fidelity model selection for variable-fidelity EM-driven design optimization of compact antennas has been addressed. By means of comprehensive numerical studies it has been demonstrated that appropriate discretization level of the low-fidelity model can be found that ensures reliable operation and low cost of the optimization algorithm. Determination of the discretization level can be aided using correlation analysis of the antenna simulated at a few designs rather than through trial and error involving complete optimization runs.

Acknowledgment

The authors would like to thank Dassault Systems, France, for making CST Microwave Studio available. This work was supported in part by the Icelandic Centre for Research (RANNIS) Grant 163299051, and by National Science Centre of Poland Grant 2015/17/B/ST6/01857.

References

[1] S. Nikolaou and M. Ali Babar Abbasi, "Design and development of a compact UWB monopole antenna with easily-controllable return loss," *IEEE Trans. Ant. Prop.*, 2017.

[2] M. Bod, H.R. Hassani, and M.M.S Taheri, "Compact UWB printed slot antenna with extra bluetooth, GSM, and GPS bands," *IEEE Ant. Wireless Prop. Lett.*, vol. 11, pp. 531-534, 2012.

[3] L. Li, S.W. Cheung, and T.I. Yuk, "Compact MIMO antenna for portable devices in UWB applications," *IEEE Trans. Antennas Prop.*, vol. 61, no. 8, pp. 4257–4264, 2013.

[4] C. Sun, Z. Wu, and B. Bai, "A novel compact wideband patch antenna for GNSS application," *IEEE Trans. Ant. Prop.*, vol. 65, no. 12, pp. 7334-7339, 2017.

[5] H. Asokan and S. Gopalakrishnan, "Inductive loaded compact monopole antenna for ultra-wideband application," *Electronics Lett.*, vol. 53, no. 15, pp. 1021-1023, 2017.

[6] M. Abbak, M.N. Akinci, A.O. Ertay, S. Ozgur, C. Isik, and I. Akduman, "Wideban compact dipole antenna for microwave imaging applications," *IET Microwaves, Ant. Prop.*, vol. 11, No. 2, pp. 265-270, 2016.

[7] M. Kushwaha and R. Kumar, "Compact coplanar waveguide-fed wideband circular polarised antenna for navigation and wireless applications," *IET Microwaves, Ant. Prop.*, vol. 9, no. 14, pp. 1533-1539, 2015.

[8] S. Zhang and G.F. Pedersen, "Compact wideband and low-profile antenna montable on large metallic surfaces," *IEEE Trans. Ant. Prop.*, vol. 65, no. 1, pp. 6-16, 2017.

[9] A. Bekasiewicz and S. Koziel, "Structure and computationally-efficient simulation-driven design of compact UWB monopole antenna," *IEEE Antennas and Wireless Prop. Lett.*, vol. 14, pp. 1282-1285, 2015.

[10] J. Liu, K.P. Esselle, S.G. Hay, and S. Zhong, "Effects of printed UWB antenna miniaturization on pulse fidelity and pattern stability," *IEEE Trans. Ant. Prop.*, vol. 62, no. 8, pp. 3093-3910, 2014.

[11] M. Koohestani, N. Pires, A.K. Skrivervik, and A.A. Moreira, "Performance study of a UWB antenna in proximity to a human arm," *IEEE Antennas and Wireless Propagation Letters*, pp. 555-558, 2013.

[12] K. Xu, Z. Zhu, H. Li, J. Huangfu, C. Li, and L. Ran, "A printed single-layer UWB monopole antenna with extended ground plane stubs," *IEEE Antennas and Wireless Propagation Letters*, pp. 237-240, 2013.

[13] L. Ghanbari, A. Keshtkar, S. Ghanbari, and S. Jarchi, "Planar low VSWR monopole antenna for UWB and LTE communication," *Mediterranean Microwave Symp. (MMS),* pp. 1-4, 2016.

[14] M. Ojaroudi, C Ghobadi, and J. Nourinia, "Small square monopole antenna with inverted T-shaped notch in the ground plane for UWB application," *IEEE Antennas Wireless Prop. Lett.,* pp. 728-731, 2009.

[15] A.A. Salih and M.S. Sharawi, "A dual-band highly miniaturized patch antenna," *IEEE Ant. Wireless Prop. Lett.*, vol. 15, pp. 1783-1786, 2016.

[16] B. Lee and F.J. Harackiewicz, "Miniature microstrip antenna with a partially filled high-permittivity substrate," *IEEE Trans. Antennas Propag.*, vol. 50, no. 8, pp. 1160–1162, Aug. 2002.

[17] S. Shi, W. Che, W. Yang, and Q. Xue, "Miniaturized patch antenna with enhanced bandwidth based on signal-interference feed," *IEEE Ant. Wireless Prop. Lett.*, vol. 14, pp. 281-284, 2015.

[18] M. Yang, Z.N. Chen, P.Y. Lau, X. Qing, and X. Yin, „Miniaturized patch antenna with grounded strips," *IEEE Trans. Ant. Prop.*, vol. 63, no. 2, pp. 843-848, 2015.

[19] S. Koziel and S. Ogurtsov, "Antenna design by simulation-driven optimization. Surrogate-based approach," Springer, 2014.

[20] J. Nocedal and S. Wright, *Numerical Optimization*, 2nd edition, Springer, New York, 2006.

[21] A.A. Al-Azza, A.A. Al-Jodah, and F.J. Harackiewicz, "Spide monkey optimization: a novel technique for antenna optimization," *IEEE Ant. Wireless Prop. Lett.*, vol. 15, pp. 1016-1019, 2016.

[22] S. Koziel, A. Bekasiewicz, "Fast EM-driven size reduction of antenna structures by means of adjoint sensitivities and trust regions," *IEEE Ant. Wireless Prop. Lett.*, vol. 14, pp. 1681-1684, 2015.

[23] D.I.L. de Villiers, I. Couckuyt, and T. Dhaene, "Multi-objective optimization of reflector antennas using kriging and probability of improvement," *Int. Symp. Ant. Prop.*, pp. 985-986, San Diego, USA, 2017.

[24] S. Koziel, S. Ogurtsov, and S. Szczepanski, "Rapid antenna design optimization using shape-preserving response prediction," *Bulletin of the Polish Academy of Sc.. Tech. Sc.*, vol. 60, no. 1, pp. 143-149, 2012.

[25] S. Koziel, "Fast simulation-driven antenna design using response-feature surrogates," *Int. J. RF & Microwave CAE*, vol. 25, no. 5, pp. 394-402, 2015.

[26] S. Koziel and S. Ogurtsov, "Model management for cost-efficient surrogate-based optimization of antennas using variable-fidelity electromagnetic simulations," *IET Microwaves Ant. Prop.*, vol. 6, no. 15, pp. 1643-1650, 2012.

[27] S. Koziel and A. Bekasiewicz, "Low-fidelity model considerations for EM-driven design of antenna structures," *J. Electromagnetic Waves App.*, vol. 30, no. 18, pp. 2444-2458, 2016.

[28] M.A. Haq, S. Koziel, and Q.S. Cheng, "EM-driven size reduction of UWB antennas with ground plane modifications," *Int. Applied Computational Electromagnetics Society (ACES China) Symposium*, 2017.

[29] T. Li, H. Zhai, G. Li, L. Li, and C. Liang, "Compact UWB band-notched antenna design using interdigital capacitance loading loop resonator," *IEEE Ant. Wireless Prop. Lett.*, vol. 11, pp. 724-727, 2012.

[30] S.K. Palaniswamy, Y. Panneer, M.G. Nabi Alsath, M. Kanagasabai, S. Kingsly, and S. Subbaraj, "3D eight-port ultra-wideband (UWB) antenna array for diversity applications," *IEEE Ant. Wireless Prop. Lett*., 2016.